Plasmonics (2013) 8:455–463
DOI 10.1007/s11468-012-9410-0

Efficient Higher Order Full-Wave Numerical Analysis of 3-D Cloaking Structures

Slobodan V. Savić · Ana B. Manić · Milan M. Ilić · Branislav M. Notaroš

Received: 28 January 2012 / Accepted: 25 June 2012 / Published online: 8 July 2012

Abstract Highly efficient and versatile computational electromagnetic analysis of 3-D transformation-based metamaterial cloaking structures based on a hybridization of a higher order finite element method for discretization of the cloaking region and a higher order method of moments for numerical termination of the computational domain is proposed and demonstrated. The technique allows for an effective modeling of the continuously inhomogeneous anisotropic cloaking region, for cloaks based on both linear and nonlinear coordinate transformations, using a very small number of large curved finite elements with continuous spatial variations of permittivity and permeability tensors and high-order *p*-refined field approximations throughout their volumes, with a very small total number of unknowns. In analysis, there is no need for a discretization of the permittivity and permeability profiles of the cloak, namely for piecewise homogeneous (layered) approximate models, with material tensors replaced by appropriate piecewise constant approximations. Numerical results show a very significant reduction (three to five orders of magnitude for the simplest possible 6-element model and five to seven orders of magnitude for an *h*-refined 24-element model) in the scattering cross section of a perfectly conducting sphere with a metamaterial cloak, in a broad range of wavelengths. Given the introduced explicit approximations in modeling of the spherical geometry and continuous material tensor profiles (both by fourth-order Lagrange interpolating functions), and inherent numerical approximations involved in the finite element and moment method techniques and codes, the cloaking effects are shown to be predicted rather accurately by the full-wave numerical analysis method.

Keywords Numerical analysis · 3-D invisibility cloaks · Transformation optics · Scattering · Metamaterials · Higher order methods

S. V. Savić · M. M. Ilić
School of Electrical Engineering, University of Belgrade,
Belgrade 11120, Serbia

A. B. Manić · M. M. Ilić · B. M. Notaroš (✉)
Department of Electrical and Computer Engineering,
Colorado State University,
Fort Collins, CO 80523-1373, USA
e-mail: notaros@colostate.edu

Introduction

In recent years, there has been great and growing interest in metamaterials, which can broadly be defined as engineered artificial composite materials exhibiting some unusual (and desirable) properties beyond "standard" or natural media (the term comes from the Greek word "meta" meaning "beyond"). These emerging materials provide tremendous opportunities for designs of new components, devices, and systems at both optical wavelengths and RF/microwave frequencies [1–7]. One important research direction in this area is based on the concept of controlling the electromagnetic (EM) fields, namely conveniently guiding and redirecting optical paths (or lines of the Poynting vector), in metamaterials designed using transformation optics (or transformation electromagnetics) techniques [8–17]. Such techniques, enabling designs of devices that possess novel wave–material interaction properties, are founded on the invariance property of Maxwell's equations under coordinate transformations. In the design process, the transformations are first employed to reshape the original coordinate system (and thus redirect the optical paths) in a desired fashion, and then, the newly formed spatial curvatures are transformed into the corresponding scaling of medium parameters (permittivity and permeability tensors).

Perhaps the best-known application of the transformation optics techniques is the design of EM/optical invisibility cloaks. There are two basic types of transformation-based metamaterial cloaks: (1) line-transformed (cylindrical) cloaks and (2) point-transformed (spherical) cloaks. In the case of line-transformed or two-dimensional (2-D) cloaks, an infinite straight line is transformed into an infinitely long spatial domain with a finite cross section of an arbitrary (designed) shape. To obtain point-transformed or three-dimensional (3-D) cloaks, on the other side, a point is transformed into a spatial domain with a finite volume of an arbitrary shape. In both cases, a goal is to have a void region (spatial region that is not spanned by any curved coordinate lines) in the new coordinate system, which is going to be invisible for observation locations outside the cloak. The first announcements of the cloaking paradigm, given in [8] and [9], rely on transformation optics and analytical (asymptotic in the geometrical optics limit) ray-tracing derivations to describe and quantify the behavior of both 2-D and 3-D cloaks. These works predict that considerable reductions in scattering cross sections of objects can be achieved, imperfect to the degree of satisfying the required derived material parameters, and they demonstrate a connection between cloaks and previously studied reflectionless interfaces such as perfectly matched layers (PMLs). They also raise important questions regarding the influence of the singularity in the ray tracing, when a ray headed directly toward the center of a cloaked sphere (or cylinder) is considered, and whether the cloaking effect is broadband or specific to a single frequency.

A great majority of more detailed studies in the field are those of 2-D cloaks [10–15]. Full-wave numerical analyses of cylindrical cloaks in [10–12] show that low reflection of a cloaking structure is not too sensitive to modest permittivity and permeability variations, that the cloaking performance degrades smoothly with increasing losses, that the effective shielding can be achieved with a cylindrical shell composed of eight piecewise homogeneous layers as an approximation of the ideal continuous medium, and that mirage effect can be observed in the structure (i.e., the source appears to radiate from a shifted location, which is in accordance with the involved geometrical transformation). A numerical study of a 2-D structured cloak, shown to work for different wavelengths provided that they are ten times larger than the size of outermost sectors of the cloaking layers, is given in [13]. Another study of cylindrical cloaks, with homogeneous and isotropic layers, can be found in [14]. An attempt to physically realize a cylindrical cloak is described in [15], where a metallic cylinder was "hidden" inside a cloak constructed from artificially structured metamaterials, designed for operation over a band of microwave frequencies. Some recent studies, based on analytical methods, investigate in more detail problems of material singularities and performances of simplified (non-exact) cloaks [16], general cloaking designs of noncircular annular geometries and the application of cloaking to RF/microwave antenna shielding [17], methodologies for cloak designs based on a linear inhomogeneous field transformation (that does not include space compression as in transformation-optics), which result in a new type of bianisotropic metamaterials that do not scatter arbitrarily incident fields [18], and cloak designs that could be implemented by silver nanowires [19]. Note that a very useful full-wave Mie scattering analytical model of spherical 3-D cloaks is given in [20]. More recently, nonlinear ("high-order") coordinate transformations have been investigated. They are introduced in order to obtain more degrees of freedom in designing the material parameters, which is essential for improving the performance of the cloak when it is approximated (segmented) into a sequence of piecewise homogeneous layers. Detailed investigations of the optimal discretization (e.g., thickness control of each layer, nonlinear factor, etc.) for both linear and nonlinear transformation-based spherical cloaks and their effects on invisibility performance are presented in [21].

However, while all the reported theoretical works and investigations of transformation-based metamaterial cloaking concepts and designs rely to greater or lesser extent on analytical derivations and analyses (based on geometrical optics or other methods), an alternative approach, a full-wave rigorous numerical analysis of 2-D, and especially 3-D, cloaking structures, based on concepts and techniques of computational electromagnetics (CEM) and guided by analytical formulas for cloaking materials, seems to have not been fully exploited. Effective numerical modeling of 3-D cloaks, in particular, would not only provide an alternative solution for spherical and other canonical shapes that can as well be analyzed analytically (e.g., using Mie's series) but would be welcome and actually unavoidable in analysis and design of more complex real-world geometries and material compositions that cannot be treated purely analytically. Of course, one should always have in mind that CEM solutions inevitably introduce some error, due to the involved modeling and numerical approximations and imperfections.

Excellent examples of 2-D numerical studies of cloaking phenomena are those in [10–12], which present full-wave simulations of cylindrical (infinitely long) cloaks using commercial COMSOL Multiphysics

software, based on a 2-D finite element method (FEM) for electromagnetic field computations. In addition, the used FEM technique relies on a piecewise homogeneous graded approximation of continuous electromagnetic parameters (permittivity and permeability) of the material, which, in turn, results in the necessity to introduce as many as 32 homogeneous material layers in the model to obtain a smooth enough approximation of the cloaking medium [10]. Finally, as electrically very small low-order finite elements are employed in the technique, it is reported that the simulation requires as many as 340,000 unknowns. A notable example of 3-D full-wave numerical analysis of spherical transformation-based cloaks appears in a study of optical nanotrapping [22], which as well is based on COMSOL Multiphysics (3-D FEM software) and reports utilization of 23,285 small cubic finite elements, domain truncation using PMLs, and 422,233 unknowns in the numerical analysis. Note that comprehensive full-wave CEM simulations of 3-D spherical plasmonic cloaks, which do not involve any anisotropy or inhomogeneity of the material, using commercial CST Microwave Studio software (based on the finite integration technique) are presented in [23].

This paper presents highly efficient and versatile full-wave rigorous 3-D numerical modeling of linear and nonlinear transformation-based spherical cloaking structures, based on a hybridization of a higher order FEM for discretization of the cloaking region and a higher order method of moments (MoM) for numerical termination of the computational domain. The cloaking region is modeled by Lagrange-type generalized curved parametric hexahedral finite elements of arbitrary geometrical orders and curl-conforming hierarchical polynomial vector basis functions of arbitrary field expansion orders for the approximation of the electric field vector within the elements [24], while the external surface of the cloak is modeled by generalized quadrilateral MoM patches in conjunction with divergence-conforming polynomial bases of arbitrary orders for the expansion of electric and magnetic equivalent surface currents over the patches [25, 26]. The FEM elements can be large and filled with anisotropic inhomogeneous materials with continuous spatial variations of complex relative permittivity and permeability tensors described by Lagrange interpolation polynomials of arbitrary material representation orders [27], so there is no need for a discretization of the permittivity and permeability profiles of the cloak, namely for piecewise homogeneous (layered) approximate models, with material tensors replaced by appropriate piecewise constant approximations (such a discretization is typical for all existing approaches to FEM analysis of transformation-based metamaterial cloaks). Furthermore, because curved elements are used, a small number of elements suffice for the geometrical precision of the model (for curvature modeling). Finally, because higher order basis functions are implemented, there is no need for a discretization of the computational domain into electrically very small elements (with low-order basis functions for field/current modeling).

Theory and Numerical Analysis Method

Consider a homogeneous isotropic medium (e.g., air) with a traveling plane wave, as shown in Fig. 1a. The light rays (or lines of the Poynting vector, **P**, of the wave) are parallel to each other. Based on the fact that Maxwell's equations are coordinate system independent, distorting the original space, with a spatial transformation applied to change the coordinate system (e.g., by employing appropriate mapping functions), will cause the rays to bend in the same manner, as depicted in Fig. 1b. Material property tensors in the transformed space, $\overline{\overline{\varepsilon}}'$ and $\overline{\overline{\mu}}'$, are related to the respective tensors in the original space $\overline{\overline{\varepsilon}}$ and $\overline{\overline{\mu}}$, via [17]:

$$\overline{\overline{\varepsilon}}' = \frac{\mathbf{J}\overline{\overline{\varepsilon}}\mathbf{J}^{\mathrm{T}}}{\det(\mathbf{J})},\ \overline{\overline{\mu}}' = \frac{\mathbf{J}\overline{\overline{\mu}}\mathbf{J}^{\mathrm{T}}}{\det(\mathbf{J})}, \tag{1}$$

where **J** stands for the 3×3 Jacobi matrix of the transformation from $\mathbf{r} = x\mathbf{i}_x + y\mathbf{i}_y + z\mathbf{i}_z$ to $\mathbf{r}' = x'\mathbf{i}'_x + y'\mathbf{i}'_y + z'\mathbf{i}'_z$, with **i** and **i**′ being the corresponding coordinate unit vectors.

A linear spherical 3-D cloak is obtained using the following linear transformation described in the spherical coordinate system with the transformation domain $0 \le r \le R_2$, $0 \le \phi < 2\pi$, and $-\pi/2 \le \theta \le \pi/2$ [8, 9]

$$r' = R_1 + \frac{R_2 - R_1}{R_2} r,\ \theta' = \theta,\ \phi' = \phi \tag{2}$$

where R_1 and R_2 are the inner and outer radii, respectively, of the spherical cloak. A cross section of the visual

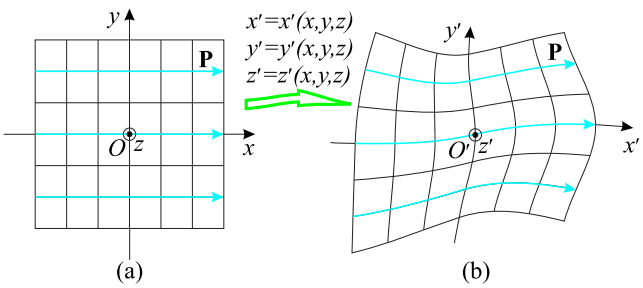

Fig. 1 An example of coordinate transformation causing deformation of light ray trajectories: **a** original rectangular coordinate system with parallel rays and **b** transformed curvilinear coordinate system with curved ray trajectories

representation of this transformation (in $z=0$ plane) is shown in Fig. 2, for the original (a) and transformed (b) coordinate systems. The region $0 \le r \le R_2$ is mapped into the spherical shell (transformation range) $R_1 \le r' \le R_2$ in the transformed coordinate system, with the Jacobi matrix of the transformation given by

$$\mathbf{J} = \begin{bmatrix} \frac{R_2 - R_1}{R_2} & 0 & 0 \\ 0 & \frac{r'}{r} & 0 \\ 0 & 0 & \frac{r'}{r} \end{bmatrix} \tag{3}$$

Substituting Eq. (3) into Eq. (1) results in the following expressions for relative permittivity and permeability tensors in the mapped space:

$$\overline{\overline{\varepsilon}}' = \overline{\overline{\mu}}' = \begin{bmatrix} \frac{R_2 (R_1 - r')^2}{(R_2 - R_1) r'^2} & 0 & 0 \\ 0 & \frac{R_2}{R_2 - R_1} & 0 \\ 0 & 0 & \frac{R_2}{R_2 - R_1} \end{bmatrix} \tag{4}$$

Finally, $\overline{\overline{\varepsilon}}'(r', \theta', \phi')$ is analytically transformed to its Cartesian equivalent (to be used in the numerical analysis) by stipulating that $\overline{\overline{\varepsilon}}'(r', \theta', \phi')\mathbf{a}'(r', \theta', \phi')$ be the same as $\overline{\overline{\varepsilon}}'(x', y', z')\mathbf{a}'(x', y', z')$, with $\mathbf{a}'$ being an arbitrary vector, and analogously for $\overline{\overline{\mu}}'$.

In addition to linear transformation 3-D spherical cloaks, two classes of nonlinear transformation 3-D spherical cloaks are introduced in [21] and classified in terms of the positive (concave up) or negative (concave down) sign of the second derivative of the transformation function. The nonlinear transformation used to construct a spherical cloak can be analytically described in the transformation domain $0 \le r \le R_2$, $0 \le \phi < 2\pi$, and $-\pi/2 \le \theta \le \pi/2$ as

$$r' = \sqrt[l]{\frac{R_2^l - R_1^l}{R_2} r + R_1^l}, \qquad \theta' = \theta, \ \phi' = \phi \tag{5}$$

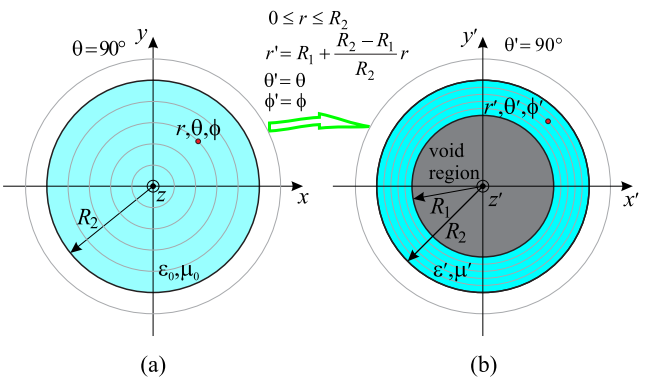

Fig. 2 Coordinate transformation yielding a spherical 3-D cloak: cross sections of **a** the original space with an air-filled homogeneous sphere and **b** the transformed space with a void region and an anisotropic continuously inhomogeneous spherical shell

for the concave up case, and as

$$r' = R_1 R_2 \sqrt[l]{\frac{R_2}{R_2^{l+1} - (R_2^l - R_1^l) r}}, \qquad \theta' = \theta, \ \phi' = \phi \tag{6}$$

for the concave down case. In both cases, l represents the degree of the nonlinearity in the transformation (l does not need to be an integer). Cartesian equivalent tensors for the relative permittivity and permeability of a nonlinear spherical cloak are derived performing algebraic manipulations analogous to those in the linear spherical cloak case. The resulting models are then used as additional examples in the evaluation of the higher order full-wave FEM-MoM technique, to demonstrate the validity of the method when more complex tensor profiles are involved.

Since r' in Fig. 2b coincides with the real radial coordinate in a spherical coordinate system attached to the center of the void region, we can now omit, for the sake of simplicity of further writing, the primes from the notation of coordinates and use (r, θ, ϕ) in place of (r', θ', ϕ').

In our full-wave 3-D computational model, the cloak is tessellated using Lagrange-type generalized curved parametric hexahedral finite elements of arbitrary geometrical orders K_u, K_v, and K_w (K_u, K_v, $K_w \ge 1$), shown in Fig. 3 and analytically described as [24]:

$$\mathbf{r}(u, v, w) = \sum_{i=0}^{K_u} \sum_{j=0}^{K_v} \sum_{k=0}^{K_w} \mathbf{r}_{ijk} L_{i,K_u}(u) L_{j,K_v}(v) L_{k,K_w}(w), \quad -1 \le u, v, w \le 1 \tag{7}$$

where $\mathbf{r}_{ijk} = \mathbf{r}(u_i, v_j, w_k)$ are position vectors of interpolation nodes and $L_{i,K_u}(u)$ represent Lagrange interpolation polynomials in the u coordinate, with u_i being the uniformly

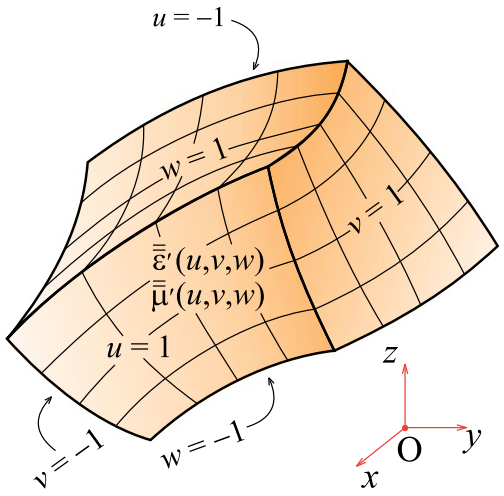

Fig. 3 Generalized curved parametric hexahedral finite element defined by Eq. (7), with continuous spatial variations of complex permittivity and permeability tensors of the material defined by Eq. (14)

spaced interpolating nodes defined as $u_i = (2i - K_u)/K_u$, $i = 0,1,\ldots,K_u$, and similarly for $L_{j,K_v}(v)$ and $L_{k,K_w}(w)$.

The electric field vector in each element, $\mathbf{E}(u,v,w)$, is approximated by means of curl-conforming (automatically satisfying the boundary condition for the tangential component of $\mathbf{E}$ at interfaces between elements) hierarchical (each lower order set of functions is a subset of all higher order sets) polynomial vector basis functions $\mathbf{f}$ as follows [24]:

$$\mathbf{E} = \sum_{m=0}^{N_u-1}\sum_{n=0}^{N_v}\sum_{p=0}^{N_w}\alpha_{umnp}\mathbf{f}_{umnp} + \sum_{m=0}^{N_u}\sum_{n=0}^{N_v-1}\sum_{p=0}^{N_w}\alpha_{vmnp}\mathbf{f}_{vmnp} + \sum_{m=0}^{N_u}\sum_{n=0}^{N_v}\sum_{p=0}^{N_w-1}\alpha_{wmnp}\mathbf{f}_{wmnp}. \quad (8)$$

The basis functions for different field components are defined by:

$$\begin{aligned}\mathbf{f}_{umnp} &= u^m P_n(v) P_p(w)\mathbf{a'}_u \\ \mathbf{f}_{vmnp} &= P_m(u) v^n P_p(w)\mathbf{a'}_v \\ \mathbf{f}_{wmnp} &= P_m(u) P_n(v) w^p \mathbf{a'}_w\end{aligned}, \quad (9)$$

$$P_m(u) = \begin{cases} 1-u, & m = 0 \\ u+1, & m = 1 \\ u^m - 1, & m \geq 2, \text{even} \\ u^m - u, & m \geq 3, \text{odd} \end{cases}$$

where the reciprocal unitary vectors $\mathbf{a'}_u$, $\mathbf{a'}_v$, and $\mathbf{a'}_w$ are obtained as

$$\mathbf{a'}_u = \frac{\mathbf{a}_v \times \mathbf{a}_w}{\Im}, \quad \mathbf{a'}_v = \frac{\mathbf{a}_w \times \mathbf{a}_u}{\Im}, \quad \mathbf{a'}_w = \frac{\mathbf{a}_u \times \mathbf{a}_v}{\Im} \quad (10)$$

from the unitary vectors $\mathbf{a}_u$, $\mathbf{a}_v$, $\mathbf{a}_w$ and the Jacobian ($\Im$) of the covariant transformation,

$$\mathbf{a}_u = \frac{\mathrm{d}\mathbf{r}}{\mathrm{d}u}, \quad \mathbf{a}_v = \frac{\mathrm{d}\mathbf{r}}{\mathrm{d}v}, \quad \mathbf{a}_w = \frac{\mathrm{d}\mathbf{r}}{\mathrm{d}w}, \quad \Im = (\mathbf{a}_u \times \mathbf{a}_v)\cdot\mathbf{a}_w \quad (11)$$

with $\mathbf{r}$ given in Eq. (7). In Eq. (8), polynomial orders N_u, N_v, and N_w (N_u, N_v, $N_w \geq 1$) are completely independent from K_u, K_v, and K_w in Eq. (7), and the basis functions are multiplied by unknown complex field distribution coefficients $\{\alpha\}$, which are determined in a numerical solution of the standard Galerkin weak-form discretization of the electric field vector wave equation

$$\int_V \bar{\bar{\mu}}^{-1}\left(\nabla \times \mathbf{f}_{\sim mnp}\right)\cdot(\nabla\times\mathbf{E})\mathrm{d}V - k_0^2\int_V \bar{\bar{\varepsilon}}\mathbf{f}_{\sim mnp}\cdot\mathbf{E}\mathrm{d}V = \mathrm{j}k_0 Z_0 \oint_S \mathbf{f}_{\sim mnp}\cdot\mathbf{n}\times\mathbf{H}\mathrm{d}S \quad (12)$$

where V is the volume of the FEM computational region (bounded by the surface S), $\mathbf{f}_{\sim mnp}$ (standing for any of the functions $\mathbf{f}_{\sim umnp}$, $\mathbf{f}_{\sim vmnp}$ or $\mathbf{f}_{\sim wmnp}$) are testing functions [the same as basis functions in Eqs. (8), (9), (10), and (11)], k_0 and Z_0 are the free-space wave number and intrinsic impedance, respectively, and $\mathbf{n}$ is the outward-looking normal on S.

Continuous spatial variations of Cartesian components of the medium tensors $\bar{\bar{\varepsilon}}'$ and $\bar{\bar{\mu}}'$ in the FEM generalized hexahedra are implemented using the same Lagrange interpolating scheme for defining element spatial coordinates in Eq. (7) [27], extended to account for different profiles in different directions. For instance, applied to the linear cloak modeling, the xx component of the Cartesian equivalent of the tensor $\bar{\bar{\varepsilon}}'$ in Eq. (4), analytically obtained to be

$$\varepsilon'_{xx}(\mathbf{r}) = \frac{x^2\varepsilon'_{rr} + (y^2+z^2)\varepsilon'_{\theta\theta}}{x^2+y^2+z^2}, \quad (13)$$

is incorporated in the FEM model as

$$\varepsilon'_{xx}(u,v,w) = \sum_{q=0}^{M_u}\sum_{s=0}^{M_v}\sum_{t=0}^{M_w}\varepsilon'_{xx,qst}L_{q,M_u}(u)L_{s,M_v}(v)L_{t,M_w}(w), \quad (14)$$

where M_u, M_v, and M_w (M_u, M_v, $M_w \geq 1$) are arbitrary material-representation polynomial orders and $\varepsilon'_{xx,qst} = \varepsilon'_{xx}(\mathbf{r}_{qst})$ are the respective relative permittivity values at the points defined by position vectors of spatial interpolation nodes, $\mathbf{r}_{qst}$, corresponding to orders M_u, M_v, and M_w, and similarly for all remaining components of $\bar{\bar{\varepsilon}}'$ and for all components of $\bar{\bar{\mu}}'$.

For the FEM mesh truncation, we introduce, in accordance to the surface equivalence principle (generalized Huygens' principle), a set of unknown electric and magnetic equivalent surface currents, $\mathbf{J}_s$ and $\mathbf{M}_s$, at the outer surface of the cloak, which are defined on curved quadrilateral patches representing external faces of the FEM hexahedra (in Fig. 3). The currents are expanded using a divergence-conforming (automatically satisfying continuity conditions for normal components of $\mathbf{J}_s$ and $\mathbf{M}_s$ at element joints) 2-D (in parametric coordinates u and v) version of FEM basis functions, with unknown current distribution coefficients being evaluated by the method of moments [25]. Scattered electric and magnetic fields due to $\mathbf{J}_s$ and $\mathbf{M}_s$ and incident fields (due to an incident plane wave) are coupled to the fields in the cloak region through boundary conditions for the tangential field components on the cloak external surface, giving rise to a hybrid higher order FEM-MoM solution [26].

Results and Discussion

Consider a spherical scatterer of diameter $d=2R_1$, situated in air, as shown in Fig. 4. The sphere is made of a perfect electric conductor (PEC) and its surface is geometrically modeled by six fourth-order $(K_u = K_v = 4)$ curved quadrilateral patches. The sphere is coated by a spherical layer (a cloak) with outer radius R_2 and relative permittivity and permeability tensors $\overline{\overline{\varepsilon}}'(r,\theta,\phi)$ and $\overline{\overline{\mu}}'(r,\theta,\phi)$ given by Eq. (4) for a linear cloak, and by the analogous expressions for a nonlinear one. We analyze the far field scattering properties of the cloaked sphere excited by a θ-polarized plane wave, incident from the direction defined by $\theta_{inc}=90°$ and $\phi_{inc}=0°$, as indicated in Fig. 4. The cloak is modeled using only six large cushion-like fourth-order $(K_u = K_v = K_w = 4)$ curved hexahedral finite elements (Fig. 4), terminated by a PEC boundary condition on the inner side $(r = R_1)$ and by six large conformal fourth-order MoM quadrilateral elements, with equivalent surface electric and magnetic currents, on the outer side $(r = R_2)$. Continuous variations of the permittivity and permeability tensor components of the cloak [e.g., Eq. (13)] are modeled within the FEM volume elements using fourth-order $(M_u = M_v = M_w = 4)$ Lagrange interpolating polynomials (where the inhomogeneity control nodes coincide with the nodes guiding the FEM element geometry). The adopted field approximation orders are $N_u = N_v = N_w = 6$ for all FEM hexahedra, which results in only 3,900 FEM unknowns (unknown field distribution coefficients). The adopted current approximation orders are $N_u = N_v = 5$ for all MoM patches, yielding a total of as few as 600 MoM unknowns (current distribution coefficients). The overall simulation takes 150 s of computational time per frequency (wavelength) point for analysis on a modest Windows 7 PC with Intel® Core™ i5 CPU 760 at 2.8 GHz and 8 GB RAM. Note that the reduction in the number of unknowns is by two orders of magnitude when compared to FEM analysis in [22], where computational times are not given.

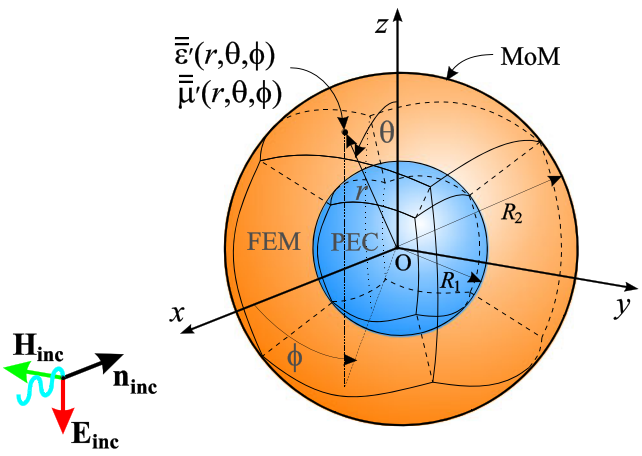

Fig. 4 FEM-MoM model of a PEC spherical scatterer with a spherical shell cloak: the cloak is modeled using only six large continuously inhomogeneous anisotropic curved finite elements with high-order polynomial field expansions in parametric coordinates

First, we assume that $R_2/R_1 = 1.1$ in Eq. (2) (a thin linear cloak) and show in Fig. 5 the normalized backscattering cross section, $\sigma/(R_1{}^2\pi)$, of the cloaked sphere obtained by the rigorous full-wave numerical FEM-MoM technique, against the normalized diameter d/λ_0 (λ_0 being the free-space wavelength) of the PEC sphere. The results include those for the lossless cloak, as well as for lossy ones with the loss tangent ranging from 0.0001 to 0.01, obtained with the original 6-element model (shown in Fig. 4) and with an *h*-refined 24-element model, where each of the 6 original elements is symmetrically subdivided into 2×2 elements along the circumferential directions. For the purpose of validation of the numerical solution, the computed scattering cross section of the uncloaked sphere, with the continuously inhomogeneous anisotropic FEM elements constituting the cloaking layer being replaced by homogeneous air-filled elements having all field and current expansions and other parameters in FEM and MoM analyses the same as in the 6-element cloak model, is also shown in Fig. 5, where it is compared with the exact Mie's series solution, and an excellent agreement of the two sets of results is observed. In addition, a fully converged *hp*-refined pure MoM solution for a homogeneous air-filled sphere,

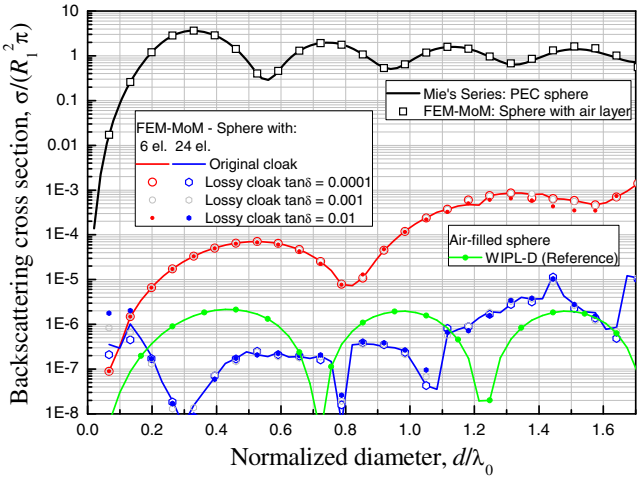

Fig. 5 Normalized backscattering cross sections of the PEC sphere with lossless and lossy linear cloaks and $R_2/R_1=1.1$ in Fig. 4, and of the uncloaked sphere, with the cloak replaced by a homogeneous air layer, obtained by the full-wave rigorous FEM-MoM numerical analysis vs. the normalized sphere diameter (λ_0 is the free-space wavelength). The uncloaked sphere is analyzed using the same six-element numerical model as the cloaked ones, and the results are compared with the exact solution in the form of Mie's series. Also shown is the backscatter of a homogeneous air-filled sphere, obtained using WIPL-D (pure MoM commercial code), as a reference for verification of the best numerical approximation of the zero backscatter from an empty spherical region of the same size as the original scatterer

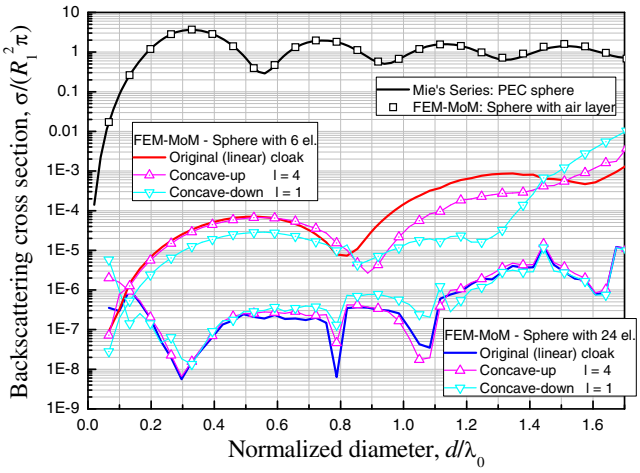

Fig. 6 Normalized backscattering cross sections of the PEC sphere with lossless nonlinear cloaks and $R_2/R_1=1.1$ in Fig. 4 computed by the higher order FEM-MoM technique vs. the normalized sphere diameter. The nonlinear cloaks include both the concave up and the concave down cases with two nonlinearity degrees in the transformations [Eqs. (5) and (6) with $l=4$ and $l=1$, respectively]. The results for the uncloaked PEC sphere and for the sphere with linear cloaks (repeated from Fig. 5) are also included for easier comparison

obtained by one of the industry's leading commercial software tools for full-wave EM analysis—WIPL-D, is shown as a reference, giving a clear insight into what the best numerical solution for the given geometry and an ideal invisibility material (scattering from free space) would be. Based on the cloaking numerical results in Fig. 5, excellent convergence properties of the method with significant reductions (three to five orders of magnitude for the 6-element model and five to seven orders of magnitude for the 24-element model, the two models being the two roughest possible) in the scattering cross section of the cloaked sphere is observed in the entire analyzed range of wavelengths, even though this is a rather thin cloak (its thickness is only one tenth of the PEC sphere radius). While having in mind that the cloak is theoretically ideal (backscatter theoretically vanishes), we note here that the (still rather rough) 24-element model yields a backscatter so low that it is on par with the best numerical approximation of the zero backscatter from an empty spherical region of the same size as the original scatterer, as verified by WIPL-D and a pure surface (MoM) model. Note also that given that some possible future applications of cloaking devices would likely include thin (for practical reasons) conformal cloaking layers on complex 3-D geometries, thin cloaks, as well as their analysis and design based on numerical simulations, rather than purely analytical methods should be of great interest in the near future. A notable example of thin cloaks based on plasmonic cloaking and scattering cancelation techniques is given in [28]. Additionally, we see in Fig. 5 that adding loss to the cloaking material practically does not influence the numerical solution for backscattering.

We next analyze a thin nonlinear cloak, based on concave up and concave down nonlinear transformations, in Eqs. (5) and (6), and for two different nonlinearity degrees, namely for $l=4$ and $l=1$, respectively, using, however, the same geometrical models, the same field and current expansions, and the same material representation orders as in the previous example (results in Fig. 5). From Fig. 6, showing the normalized backscattering cross section of the cloaked PEC sphere, we observe that the higher order FEM-MoM simulation results for the nonlinear cloaks match the results for the linear cloaks very well and, hence, that the proposed analysis method can handle nonlinear coordinate transformations equally well, without the necessity to

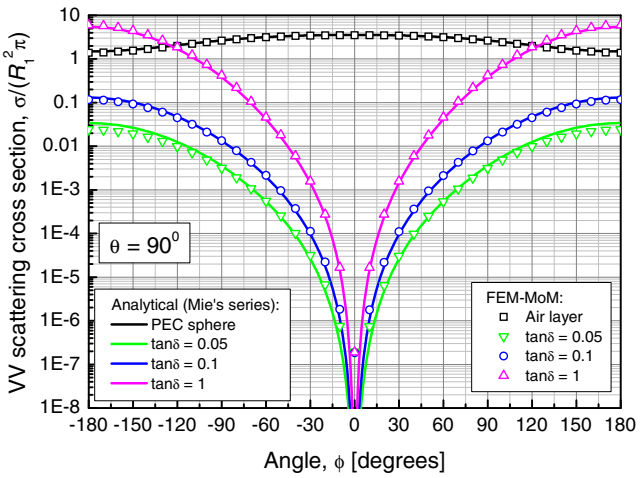

Fig. 7 Normalized VV scattering cross section of the cloaked and uncloaked PEC sphere in Fig. 4 for lossy linear cloaks, with $R_2/R_1=1.5$ and the normalized sphere diameter of $d/\lambda_0=0.3$

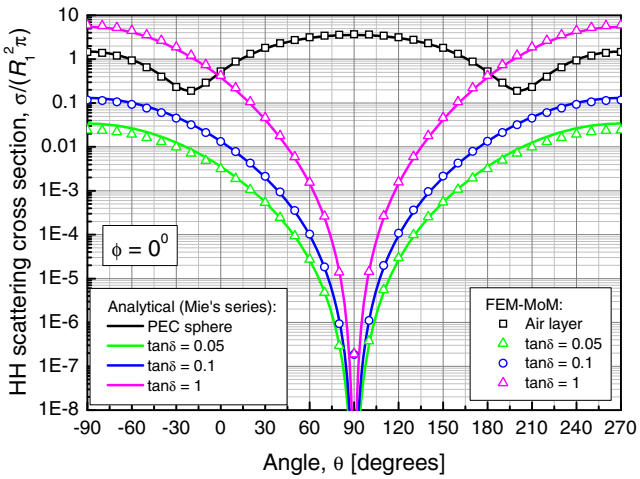

Fig. 8 Normalized HH scattering cross section of the structure in Fig. 4 (lossy linear cloaks, $R_2/R_1=1.5$, and $d/\lambda_0=0.3$)

subdivide the mesh or introduce piecewise constant (e.g., layered) material regions. We also remark that in cases where the nonlinearity of the transformation is even more pronounced, material representation polynomials of orders higher than four (orders $M_u = M_v = M_w = 4$ are found to be sufficient in the presented examples) can be employed in Eq. (14) to allow for a more adequate Lagrange interpolation of the more pronounced continuous change of media parameters within large FEM elements.

As the last example, we adopt $R_2 = 1.5R_1$ in Eq. (2) (a thicker linear cloak) and show in Figs. 7 and 8 the normalized scattering cross sections of the PEC sphere with and without lossy cloaks, respectively, for the normalized sphere diameter of $d/\lambda_0 = 0.3$, in two characteristic planes. The simplest six-element models (Fig. 4) are used for the simulations. For the cloaks with the loss tangent ranging from 0.05 to 1, numerical results are compared to exact Mie's series solutions obtained as presented in [20]. A very substantial reduction (three to seven orders of magnitude) in σ achieved by the cloak is observed, with an excellent agreement of numerical and analytical solutions for all scattering angles except for those approaching the backscattering angle (appearing in the middle of each of the graphs), at which the scattering cross section theoretically vanishes. However, we realize that all numerical backscatter solutions are practically the same, regardless of loss, and again identify the lowest cross section limit that the code and the adopted model and single machine precision can numerically achieve in this example. Note, however, that the predicted backscatter is approximately two orders of magnitude lower than that for the thin cloak for the same particle electrical size and the same simple FEM-MoM model, namely $\sigma/\left(R_1^2\pi\right) \approx 2 \times 10^{-7}$ for the thick cloak vs. $\sigma/\left(R_1^2\pi\right) \approx 3.5 \times 10^{-5}$ for the thin one, implying that thicker cloaks are numerically easier to solve, which, in turn, may be attributed to longer paths for the fields to relax.

Conclusions

This paper has proposed and demonstrated a highly efficient and versatile 3-D numerical model of a cloaking structure. In particular, it has presented higher order FEM-MoM computational electromagnetic analysis of linear and nonlinear transformation-based metamaterial spherical cloaks, with the continuously inhomogeneous anisotropic cloaking region modeled using large curved finite elements that allow continuous spatial variations of complex permittivity and permeability tensors and high-order field approximations throughout their volumes. The flexibility of the technique has enabled a very effective modeling of the cloak by means of only six FEM elements and six MoM patches over the volume and external surface, respectively, of the cloaking layer, and a very small number of unknowns. Numerical results have shown a very significant reduction (three to five orders of magnitude for a 6-element model and five to seven orders of magnitude for a 24-element model) in the scattering cross section of the cloaked PEC sphere in a quite broad range of wavelengths. Given the introduced explicit approximations in modeling of the spherical geometry and continuous material tensor profiles (both by fourth-order Lagrange interpolating functions), and inherent numerical approximations involved in the FEM and MoM techniques and codes, a conclusion is that the cloaking effects can be predicted rather accurately by the presented full-wave numerical analysis method. The method and numerical model can be readily adapted for analysis and design of electrically larger and/or more complex 3-D cloaking devices (which can be arbitrarily inhomogeneous and can include sharp edges and reentrant corners) with proper *h*, *p*, and *hp* refinements [29] of simple initial models.

Acknowledgments This work was supported by the National Science Foundation under grants ECCS-0650719 and ECCS-1002385 and by the Serbian Ministry of Science and Technological Development under grant TR-32005.

References

1. Alù A, Engheta N (2011) Optical metamaterials based on optical nanocircuits. Proc IEEE 99(10):1669–1681. doi:10.1109/JPROC.2011.2160834
2. Engheta N, Ziolkowski RW (eds) (2006) Metamaterials: physics and engineering explorations, 1st edn. Wiley-IEEE Press, New York
3. Christophe C, Tatsuo I (2005) Electromagnetic metamaterials: transmission line theory and microwave applications, 1st edn. Wiley-IEEE Press, New York
4. Capolino F (2009) Metamaterials handbook, 1st edn. CRC Press, New York
5. Cai W, Shalaev VM (2010) Optical metamaterials: fundamentals and applications, 1st edn. Springer, New York
6. Pendry JB (2004) Negative refraction. Contemp Phys 45(3):191–202. doi:10.1080/00107510410001667434
7. Scherer A, Painter O, Vuckovic J, Loncar M, Yoshie T (2002) Photonic crystals for confining, guiding, and emitting light. IEEE Trans Nanotechnol 1(1):4–11. doi:10.1109/TNANO.2002.1005421
8. Pendry JB, Schurig D, Smith DR (2006) Controlling electromagnetic fields. Science 312(5781):1780–1782. doi:10.1126/science.1125907
9. Schurig D, Pendry JB, Smith DR (2006) Calculation of material properties and ray tracing in transformation media. Opt Express 14 (21):9794–9804. doi:10.1364/OE.14.009794

10. Cummer SA, Popa B-I, Schurig D, Smith DR, Pendry J (2006) Full-wave simulations of electromagnetic cloaking structures. Phys Rev E 74(3):036621. doi:10.1103/PhysRevE.74.036621
11. Zolla F, Guenneau S, Nicolet A, Pendry JB (2007) Electromagnetic analysis of cylindrical invisibility cloaks and the mirage effect. Opt Lett 32(9):1069–1071. doi:10.1364/OL.32.001069
12. Ni Y, Gao L, Qiu C-W (2010) Achieving invisibility of homogeneous cylindrically anisotropic cylinders. Plasmonics 5(3):251–258. doi:10.1007/s11468-010-9145-8
13. Farhat M, Guenneau S, Movchan AB, Enoch S (2008) Achieving invisibility over a finite range of frequencies. Opt Express 16 (8):5656–5661. doi:10.1364/OE.16.005656
14. Huang Y, Feng Y, Jiang T (2007) Electromagnetic cloaking by layered structure of homogeneous isotropic materials. Opt Express 15(18):11133–11141. doi:10.1364/oe.15.011133
15. Schurig D, Mock JJ, Justice BJ, Cummer SA, Pendry JB, Starr AF, Smith DR (2006) Metamaterial electromagnetic cloak at microwave frequencies. Science 314(5801):977–980. doi:10.1126/science.1133628
16. Yan M, Yan W, Qiu M (2009) Invisibility cloaking by coordinate transformation. In: Emil W (ed) Progress in optics, vol 52., pp 261–304. doi:10.1016/s0079-6638(08)00006-1
17. Kwon D-H, Werner DH (2010) Transformation electromagnetics: an overview of the theory and applications. IEEE Antenn Propag Mag 52(1):24–46. doi:10.1109/MAP.2010.5466396
18. Maci S (2010) A cloaking metamaterial based on an inhomogeneous linear field transformation. IEEE Trans Antenn Propag 58 (4):1136–1143. doi:10.1109/TAP.2010.2041272
19. Xie Y, Chen H, Xu Y, Zhu L, Ma H, Dong J-W (2011) An invisibility cloak using silver nanowires. Plasmonics 6(3):477–481. doi:10.1007/s11468-011-9226-3
20. Chen H, Wu B-I, Zhang B, Kong JA (2007) Electromagnetic wave interactions with a metamaterial cloak. Phys Rev Lett 99 (6):063903. doi:10.1103/PhysRevLett.99.063903
21. Qiu C, Hu L, Zhang B, Wu B-I, Johnson SG, Joannopoulos JD (2009) Spherical cloaking using nonlinear transformations for improved segmentation into concentric isotropic coatings. Opt Express 17(16):13467–13478. doi:10.1364/OE.17.013467
22. Furlani EP, Baev A (2009) Optical nanotrapping using cloaking metamaterial. Phys Rev E 79(2):026607. doi:10.1103/PhysRevE.79.026607
23. Alù A, Engheta N (2007) Plasmonic materials in transparency and cloaking problems: mechanism, robustness, and physical insights. Opt Express 15(6):3318–3332. doi:10.1364/OE.15.003318
24. Ilić MM, Notaroš BM (2003) Higher order hierarchical curved hexahedral vector finite elements for electromagnetic modeling. IEEE Trans Microw Theor Tech 51(3):1026–1033. doi:10.1109/TMTT.2003.808680
25. Djordjević M, Notaroš BM (2004) Double higher order method of moments for surface integral equation modeling of metallic and dielectric antennas and scatterers. IEEE Trans Antenn Propag 52 (8):2118–2129. doi:10.1109/TAP.2004.833175
26. Ilić MM, Djordjević M, Ilić AŽ, Notaroš BM (2009) Higher order hybrid FEM-MoM technique for analysis of antennas and scatterers. IEEE Trans Antenn Propag 57(5):1452–1460. doi:10.1109/TAP.2009.2016725
27. Ilić MM, Ilić AŽ, Notaroš BM (2009) Continuously inhomogeneous higher order finite elements for 3-D electromagnetic analysis. IEEE Trans Antenn Propag 57(9):2798–2803. doi:10.1109/TAP.2009.2027350
28. Guild MD, Haberman MR, Alù A (2011) Plasmonic cloaking and scattering cancelation for electromagnetic and acoustic waves. Wave Motion 48(6):468–482. doi:10.1016/j.wavemoti.2011.02.006
29. Notaroš BM (2008) Higher order frequency-domain computational electromagnetics. IEEE Trans Antenn Propag 56(8):2251–2276. doi:10.1109/TAP.2008.926784